Supporting Information

Combined effect of heat shock protein inhibitor geldanamycin and free radicals on photodynamic therapy of prostate cancer

Qinyan Sun[a], Fengyu Liu[b,*], Zhenfu Wen[a], Jing Xia[a], Hongjuan Li[a], Yongqian Xu[a], Shiguo Sun[a,c,*]

[a]Shaanxi Key Laboratory of Natural Products & Chemical Biology, College of Chemistry & Pharmacy, Northwest A&F University, Xinong Road 22, Yangling, Shaanxi 712100, China

[b]State Key Laboratory of Fine Chemicals, School of Chemistry, Dalian University of Technology, No. 2 Linggong Road, Ganjingzi District, Dalian 116023, China

[c]College of Chemistry and Pharmaceutical Engineering, Hebei University of Science and Technology, Shijiazhuang 050018, China.

*Corresponding authors:

*Email: Prof. Shiguo Sun (sunsg@nwsuaf.edu.cn)

Prof. Fengyu Liu (liufengyu@dlut.edu.cn)

ORCID: Shiguo Sun: http://orcid.org/0000-0003-3135-8542

Fengyu Liu: https://orcid.org/0000-0002-1839-2343

Experimental Section

Materials

2-methylimidazole (2-MIM, 98%) and Geldanamycin (17-AAG, 97%) were purchased from Meryer (Shanghai, China). 2,2-azobis[2-methoxy-N-(2-hydroxy ethyl) propinamide] ($C_{12}H_{24}N_4O_4$, V-086, 98%) were purchased from Macklin (Shanghai, China). 2,2'-azobis(2-methylpropionamidine) dihydrochloride ($C_8H_{20}C_{l2}N_6$, V-50, 98%), 2,2′-azobis[2-(2-imidazolinI-2-yl) propane]dihydrochloride ($C_{12}H_{24}C_{l2}N_6$, AIBI, 98%), Hyaluronic acid (HA, 97%) and Indocyanine green (ICG, 95%) were purchased from Energy Chemical (Shanghai, China). 3-[4,5-dimethylthialzol-2-yl]-2,5-diphenyltetrazolium bromide (MTT), dimethyl sulfoxide (DMSO), monopotassium phosphate (KH_2PO_4), potassium chloride (KCl), sodium chloride (NaCl), and disodium hydrogen phosphate (Na_2HPO_4) are analytical grade and obtained from Sigma-Aldrich (Shanghai, China). The Hsp90, Survivin, and AR ELISA kit were purchased from Jiangsu Meimian Industrial Co., Ltd, China. All chemicals were used as received without any further purification. All aqueous solutions were prepared with ultrapure Milli-Q water ($\rho > 18.0$ MΩ/cm).

Measurement

UV–visible spectra were obtained on a Shimadzu 1750 UV–visible spectrometer. The size distribution and zeta potential of various nanoparticles were investigated by dynamic light scattering (DLS) with a ZEN3600 (MALVERN INSTRUMENTS LIMITED, UK). Thermogravimetric Analysis (TGA) was carried out on TGA/DSC 3+ (Switzerland). Cell toxicity tests were tested by a microplate reader (KHB ST-360, Shanghai). A Quanta 200 environmental scanning electron microscope (SEM) (Nova Nano SEM–450) was used to observe the morphologies of the obtained materials. Transmission electron microscope (TEM) images were recorded with a TECNAI G2 SPIRIT BIO transmission electron microscope operating at 200 kV. Use BD FACSAria™ III flow cytometer to study cell uptake ability. The images were acquired using a confocal fluorescence microscope (REVOLUTION WD).

Calculation methods

The geometric configuration of the intermediate state transition was assessed using the Gauss View composition software to construct the initial transition state configuration. Gaussian 09 program was used to optimize the structure and calculate the frequency of the initial transition state configuration on the level of RB3LYP/6-31g (d)[1] level, and the transition state configuration was obtained. Frequency analysis confirmed that the calculated configuration was the intermediate transition state of the reaction. Then, at the same method level, the reaction process was analyzed by intrinsic reaction coordinate (IRC) to obtain the molecular configuration of the reactants and products.

Preparation of the A/I@aZIF (AIZ) NPs

A/I@aZIF (AIZ) NPs was synthesized according to the previous work.[2] First, 1.1 g of 2-MIM was dissolved in 40 mL of H_2O, and 100 mg of $Zn(NO_3)_2 \cdot 6H_2O$ was dissolved in 4 mL of H_2O. After that, 64.4 mg AIBI and 5 mg ICG were dissolved in 2 mL H_2O, the stock solution (2 mL) of AIBI and ICG were added to the solution of $Zn(NO_3)_2 \cdot 6H_2O$. After Stirring for 5 min, the mixed solution was added dropwise to the 2-MIM solution while stirring. After stirring for 30 min, precipitation can be obtained using a centrifuge, which was then washed with water more than three times to eliminate the unreacted reactants. AIZ NPs were obtained after freeze-drying. SEM and TEM tests were prepared by redispersing some products into water. Moreover, I@aZIF (IZ) NPs were similarly synthesized for comparison using 2 mL (2.5 mg/mL) ICG stock solutions.

The drug loading content (LC) was calculated according to the following equation: Loading content = ((total amount of drug – the amount of free drug in the supernatant)/ (Weight of nanoparticles)) × 100%.[3]

Loading the AIZ NPs with 17-AAG

40 mg AIZ NPs were dissolved in 2 mL of water and dispersed by ultrasound. Then, a 0.5 mg/mL 17-AAG solution was slowly added dropwise to the solution and stirred for 12 h. Finally, the obtained product was collected by centrifugation, and then washed with water (pH=7.4) twice to get A/I@aZIF@AAG (AIZA) NPs .

Synthesis of A/I@aZIF@AAG@HA (AIZAH) NPs

HA-functionalized AIZA NPs (defined as A/I@aZIF@AAG@HA (AIZAH) NPs) were obtained as follows. Moderate amounts of HA were dissolved in 50 mL water (pH=7.4) with the assistance of the ultrasonic treatment process. Then, AIZA NPs obtained in the previous step were added dropwise to the HA solution with vigorous stirring for 41 h at room temperature. Finally, the resulting product was collected by centrifugation, which was then washed with water (pH=7.4) more than three times to eliminate the unreacted reactants.

Generation of $ABTS^{+\bullet}$ free radicals

The aqueous mixture of ABTS (2 mg/mL) and AIZAH NPs (2 mg/mL) was kept for 2, 4, and 5 h at 37 or 45 ºC in the dark. Then, the absorbance of the $ABTS^{+\bullet}$ solution was recorded with a UV–visible spectrophotometer.

In vitro ROS detection

1,3-Diphenylisobenzofuran (DPBF) was used for in vitro detection of ROS. The DPBF solution (10 μL, 10 mM in DMSO) was added to the sample solution under irradiation (808 nm, 0.5 W cm^{-2}), and the absorbance of the DPBF solution was recorded at 420 nm every two minutes.

Photothermal performance measurements

The AIZAH NPs solution (200 μg/mL, ICG concentration: 17 μg/mL), free ICG dispersion (ICG concentration: 17 μg/mL), and AIBI dispersion (200 μg/mL) were measured upon 808 nm laser irradiation (1 W cm^{-2}) for 600 s, respectively. The control group was also performed with DI water. A thermocouple probe was used to obtain the temperatures every 20 seconds. Subsequently, various concentrations of AIZAH NPs solution (50, 165, 200, and 400 μg/mL, respectively) were performed under 808 nm NIR irradiation at 1.0 W cm^{-2} for 600 s. To investigate the influence of power density on the photothermal effect, AIZAH NPs solution (200 μg/mL) was exposed to different power densities of 0.5, 1.0, 1.5 W cm^{-2} for 600 s, respectively. The photothermal stability of AIZAH NPs solution and free ICG solution was characterized by on/off irradiation for recording the temperature change curves and the repeated heating-cooling cycles. Briefly, the suspension was first irradiated for 600 s, followed by natural cooling for 600 s, and this was alternately for 4 cycles. In detail, 3 mL aqueous

dispersions of the samples were exposed to a continuous-wave diode NIR irradiation for 600 seconds over a range of concentrations in a quartz cuvette. The laser spot was focused on the center of the sample. The solution temperature was dynamically recorded using a digital thermometer (precision: 0.1 ºC) with a thermocouple probe at intervals of 10 s during NIR irradiation.

ICG and 17-AAG controlled release from AIZAH NPs

The samples dispersed in PBS buffer solutions with different pH values (7.4 and 5.0) were placed in a 37 ºC water bath, protected from light, and gently shaken. At different times, collect samples from glass bottles and centrifuge at 10000 rpm for 10 min. Then, a UV–visible spectrometer is used to determine the amount of ICG and 17-AAG that were released. All release experiments were carried out three times.

Cell culture

In a humidified atmosphere of 5% CO_2 and 21% O_2 as the normoxic condition., LNCaP (human prostate carcinoma cell line) cells were cultured at 37 ºC in RPMI 1640 medium with 10 v/v% fetal bovine serum (FBS) and 1 v/v% antibiotic and 1% v/v% Glutamax and 1% Sodium pyruvate. RWPE-1 cells (human prostate normal liver cell line) were cultured at 37 ºC in Keratinocyte medium supplemented with recombinant epidermal growth factor (rEGF) and bovine pituitary extract (BPE). HL7702 cells (human normal liver cells) were cultured at 37 ºC in RPMI 1640 medium supplemented with 10 v/v% FBS and 1 v/v% antibiotic (complete 1640). For cell passage, 0.25% trypsin solution was used to digest the cells. The corresponding 96-well plate or confocal culture dish was placed in a hypoxic environment instead of using hypoxic cell culture media. Hypoxic microenvironment (~ 0.1% O_2, 5% CO_2) was maintained by using the Anaero Pouch system for cell culture. Fig S1 shows that the hypoxic environment is caused by placing the Anaero Pouch, oxygen indicator and the cell culture dish together. When the oxygen content is greater than 0.5%, the indicator is blue. While the oxygen content is less than 0.1%, the indicator is pink.

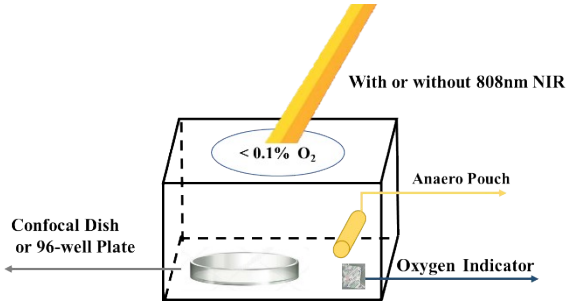

Fig S1 Schematic diagram of maintaining hypoxic environment

Cellular Uptake

LNCaP or RWPE-1 cells were seeded into the cell culture dish and treated with AIZAH NPs for different durations. Then, the cells were added Hoechst 33342 dye (excitation wavelengths were 405nm and receiving wavelengths were: 447±60nm) for 10 min to label the nucleus. Finally, the cells were washed thoroughly with PBS (pH =7.4) before imaging using a confocal laser scanning microscope. ICG excitation wavelength was 630nm and receiving wavelengths were:684±40nm.

Cell viability

Cytotoxicity of NPs was evaluated against LNCaP, RWPE-1, and HL7702 cells at different concentrations by a typical MTT assay. LNCaP, RWPE-1, and HL7702 cells were seeded into a 96-well plate at a density of 1×10^4 cells per well and cultured for 24 h, Then different concentrations of NPs were added. After 24 h incubation, a fresh medium containing MTT (0.5 mg/mL) was added to each well. After another 4 h of incubation, the MTT containing medium was removed, and DMSO (100 μL) was added to each well to dissolve the formazan crystals. Finally, the plate was gently shaken for 10 min, and the absorbance was recorded at 490 nm using a microplate reader.

Intracellular reactive oxygen species (ROS) assay

LNCaP cells were cultured with I@aZIF@AAG@HA (IZAH) NPs or AIZAH NPs at ICG concentration of 8 μg/mL for 6 h. Then, Cells were incubated with DCFH-DA (10 μM) for 20 min at 37 ºC in the dark. Cells were then irradiated with 808 nm laser for 10 min at 1.0 W cm^{-2}. Cells were washed with PBS three times, and CLSM monitored ROS generation. DCF decomposed from DCFH-DA was excited at 488 nm, and fluorescence was detected from 500 to 550 nm.

In Vitro Synergic Therapeutic Efficacy and Cytotoxicity Assay

Cell viabilities were evaluated by MTT assay and the detailed procedure as described in the above section 2.12. LNCaP cells were incubated for 24 h with various samples at different concentrations. To evaluate the synergic therapeutic efficiency, after 4 h of incubation, cells were irradiated with NIR irradiation (808 nm, 1.0 W cm^{-2}, 10 min) and then incubated for a further 20 h.

Protein content Evaluation

Survivin protein, Hsp90, and AR were measured by ELISA. Quantitative levels of Survivin, Hsp90, and AR protein were obtained to control or treated LNCaP cells using the human Total Survivin, Hsp90, and AR protein ELISA kit. Protein concentrations were determined from cell lysates, and the survivin content was calculated per pg of the total protein. All data were expressed as the mean values ± standard deviations from 4 separate experiments in each group.

Table S1 List of Abbreviations in This Work.

Full Name	Abbreviations	Full Name	Abbreviations
Photodynamic Therapy	PDT	Reactive Oxygen Species	ROS
Indocyanine green	ICG	2,2’-azobis[2-(2-imidazolinI-2-yl) propane] dihydrochloride	AIBI
Heat Shock Protein 90	Hsp90	Geldanamycin	17-AAG
Anti-apoptotic Proteins	survivin	Androgen Receptor	AR
2,2'-azobis(2-methylpropionamidine) dihydrochloride	V-50	2,2-azobis[2-methoxy-N-(2-hydroxy ethyl)] propinamide	V-086
A/I@aZIF	AIZ	A/I@aZIF@AAG@HA	AIZAH
Hyaluronic Acid	HA	A/I@aZIF@AAG	AIZA
2′,7′-dichlorodihydrofluorescein diacetate	DCFH-DA	I@aZIF@AAG@HA	IZAH
A/I@aZIF@HA	AIZH	I@aZIF@HA	IZH

Sort by time of first appearance in the manuscript

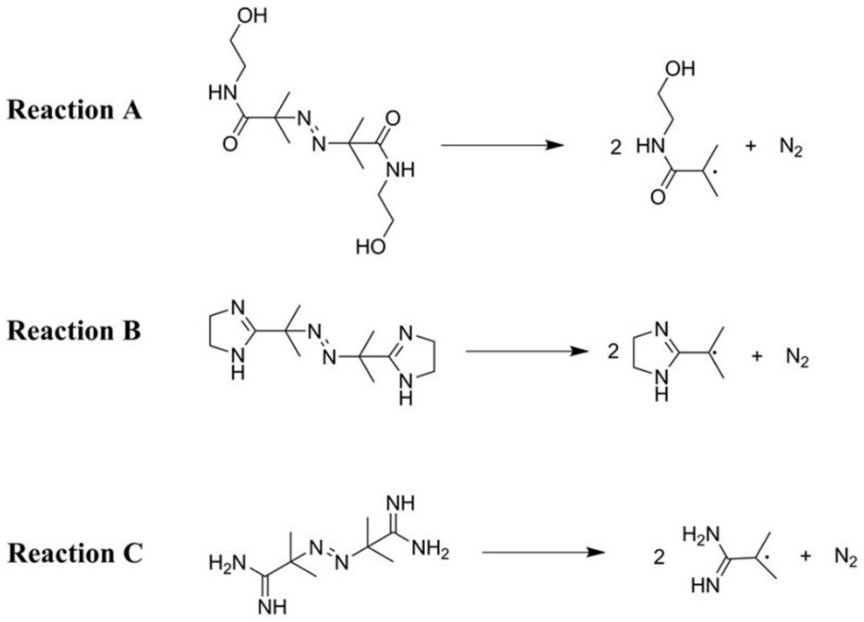

Fig. S2 The decomposition reaction process of three commercial initiators.

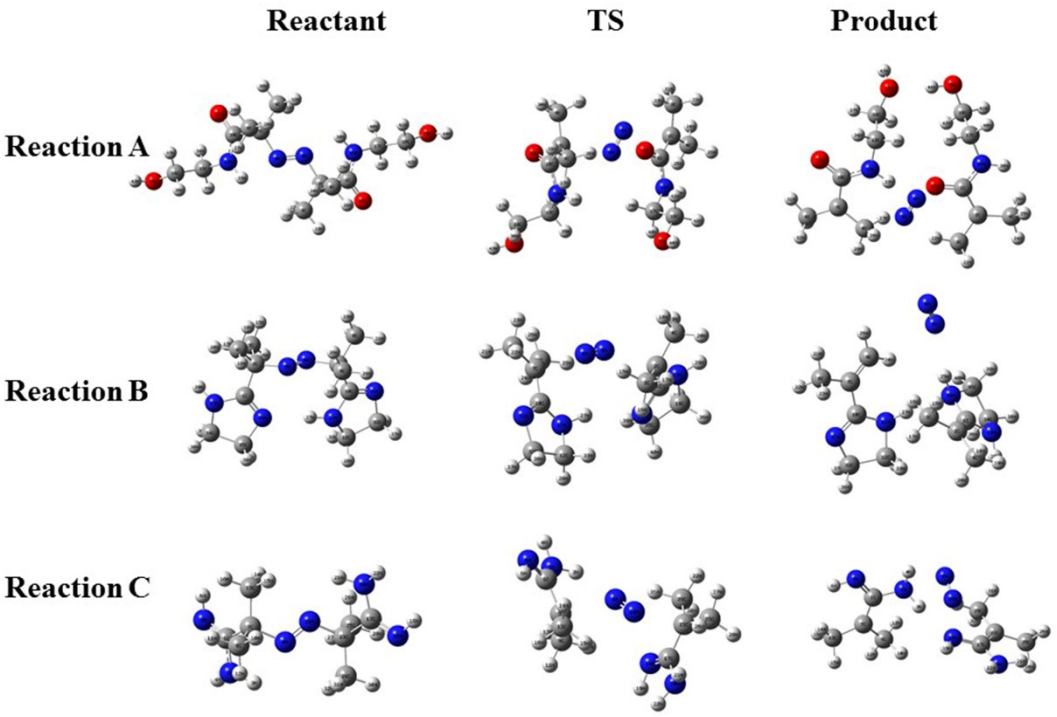

Fig. S3 Geometry of reactants, intermediate transition states and products. (Blue represents N atoms, red represents O atoms, gray represents C atoms, and white represents H atoms).

V-086

reactant		transition state		product	
7C-8N	1.49828	7C-8N	2.20321	7C-8N	5.52659
23C-24N	1.49954	23C-24N	2.29062	23C-24N	4.9163
8N-24N	1.23633	8N-24N	1.13719	8N-24N	1.10533
∠7C-8N-24N	115.368	∠7C-8N-24N	113.617	∠7C-8N-24N	92.466
∠23C-8N-24N	114.826	∠23C-8N-24N	107.449	∠23C-8N-24N	98.736
∠7C-8N-24N-23C	-178.836	∠7C-8N-24N-23C	143.561	∠7C-8N-24N-23C	62.99

AIBI

reactant		transition state		product	
7C-6N	1.49821	7C-6N	2.21694	7C-6N	5.17589
2C-5N	1.49747	2C-5N	2.29766	2C-5N	4.55808
5N-6N	1.23744	5N-6N	1.13814	5N-6N	1.10501
∠2C-5N-6N	113.819	∠2C-5N-6N	109.627	∠2C-5N-6N	141.364
∠7C-6N-5N	114.339	∠7C-6N-5N	110.311	∠7C-6N-5N	54.359
∠2C-5N-6N-7C	-177.085	∠2C-5N-6N-7C	-146.866	∠2C-5N-6N-7C	-88.405

V-50

reactant		transition state		product	
2C-5N	1.48767	2C-5N	2.29353	2C-5N	4.65522
7C-6N	1.48766	7C-6N	2.35479	7C-6N	5.28128
5N-6N	1.23884	5N-6N	1.13	5N-6N	1.10527
∠7C-6N-5N	115	∠7C-6N-5N	106.7	∠7C-6N-5N	42.1
∠6N-5N-2C	115	∠6N-5N-2C	115.2	∠6N-5N-2C	88.8
∠7C-6N-5N-2C	178	∠7C-6N-5N-2C	143	∠7C-6N-5N-2C	82.4

Fig. S4 Parameter of different reaction of reactant, product and transition state.

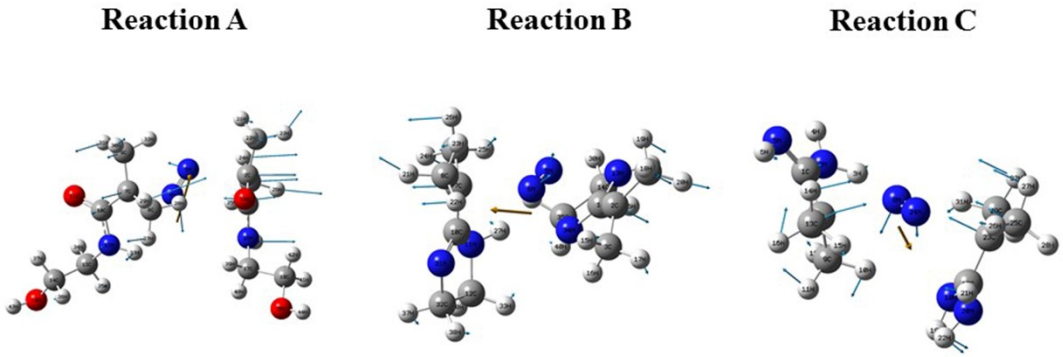

Fig. S5 Vibration modes of transition states for different reactions. (Blue represents N atoms, red represents O atoms, gray represents C atoms, and white represents H atoms).

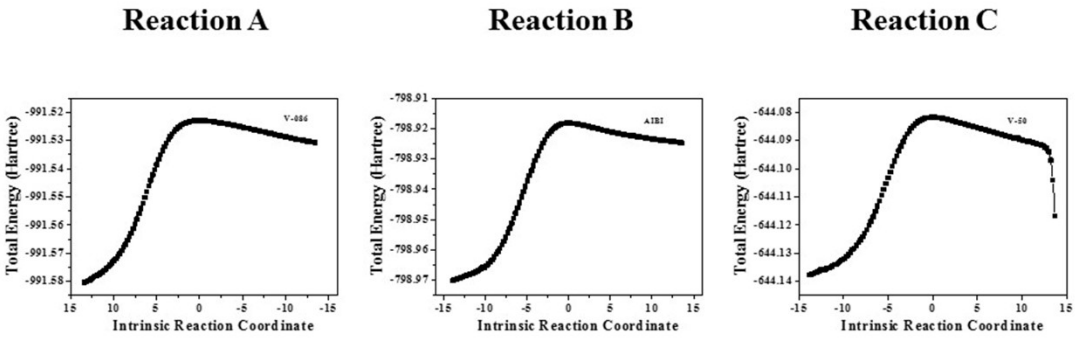

Fig. S6 Curve of reaction potential energy for different reactions.

		Total energy /Hartree	Ea/(Kcal/mol)
Reaction A (V-086)	Reactant	-991.59831320	47.28
	TS	-991.52296798	
	Product	-991.59064505	
Reaction B (AIBI)	Reactant	-798.97790197	37.45
	TS	-798.91822682	
	Product	-799.01128067	
Reaction C (V-50)	Reactant	-644.14680311	40.78
	TS	-644.08181712	
	Product	-644.13432057	

Fig. S7 The activation energy (Ea) of the forward reaction of each reaction.

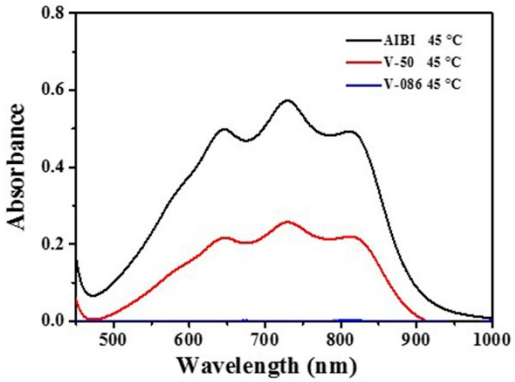

Fig. S8 Generation of $ABTS^{+\bullet}$ as induced by the free radicals released from AIBI, V-50 and V-086 at 45 °C.

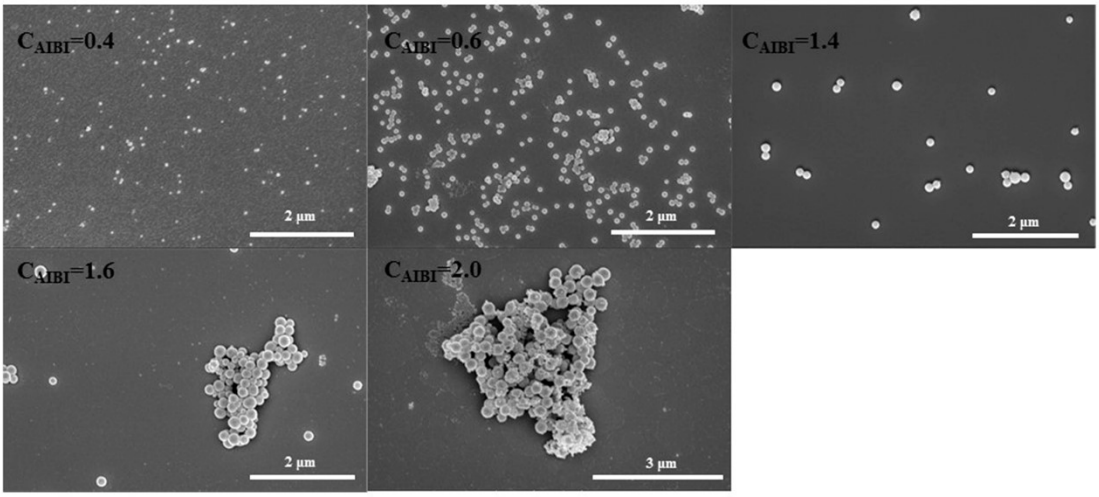

Fig. S9 Image of AIZ NPs with different concentrations of AIBI (C_{AIBI}=0.4, 0.6, 1.4, 1.6, 2.0 mg/mL).

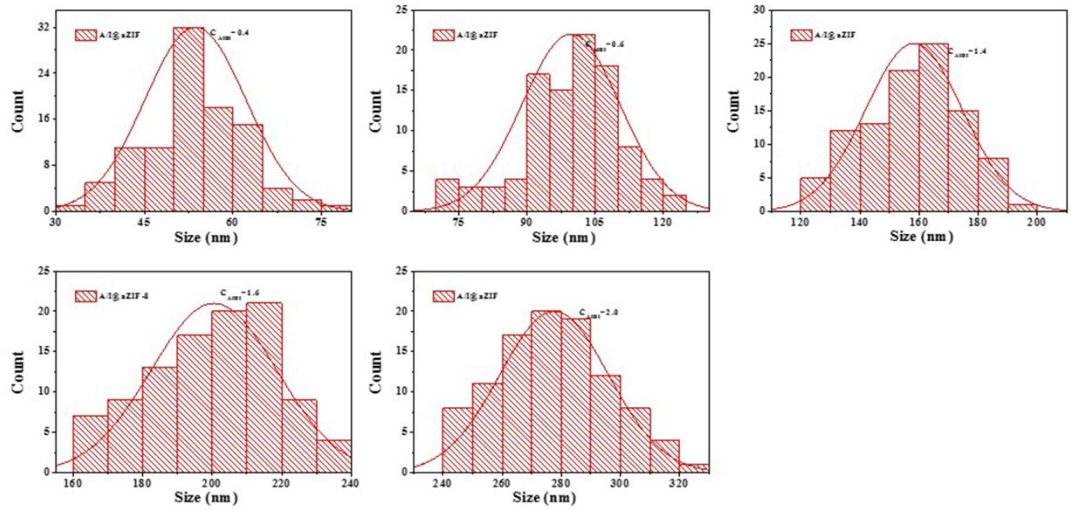

Fig. S10 Size distribution of the as-prepared AIZ NPs (C_{AIBI}=0.4, 0.6, 1.4, 1.6, 2.0 mg/mL).

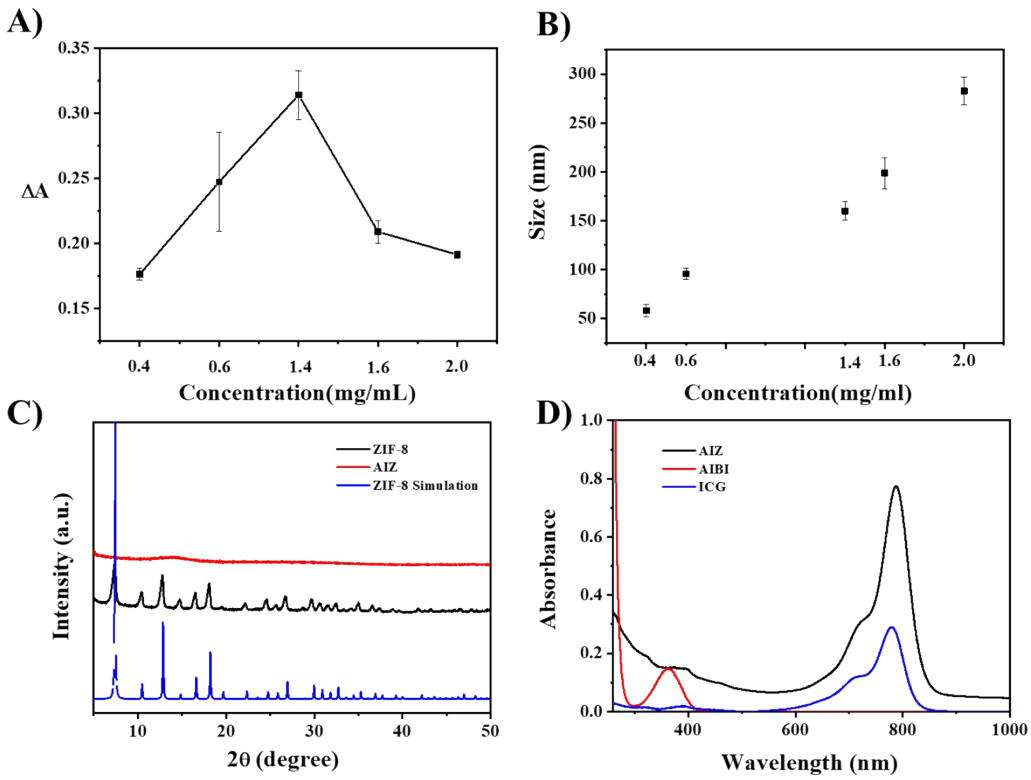

Fig. S11 A) Changes in the absorbance spectra of $ABTS^{+\bullet}$ induced changes by free radicals from AIZ NPs with different concentrations of AIBI. B) The particle size of AIZ NPs corresponding to different concentrations of AIBI. All data points represent as mean ± s.d. (n=20). C) X-ray diffraction (XRD) patterns of simulated ZIF-8, ZIF-8, AIZ NPs. D) UV–visible absorption spectra of ICG, AIBI dissolved in water, and AIZ NPs dispersed in water.

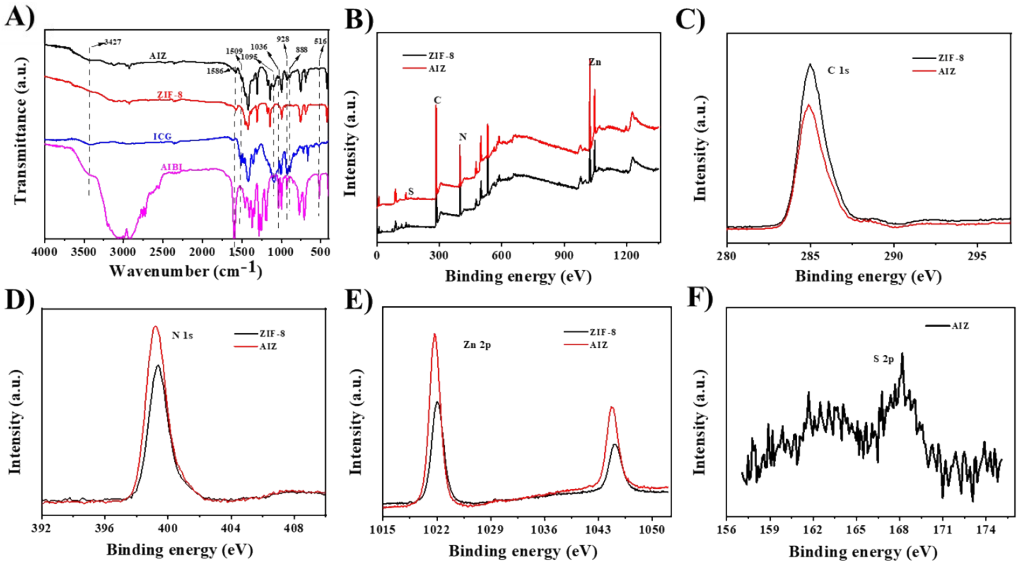

Fig. S12 A) FT-IR spectra of AIZ NPs in comparison with that of ZIF-8, AIBI and ICG. B) XPS spectra (full). XPS spectra of ZIF-8 and AIZ NPs. C) High-resolution XPS spectra. XPS spectra of C1) C 1s spectrum; C2) N 1s spectrum ; C3) Zn 2p spectrum and C4) S 2p spectrum of various samples.

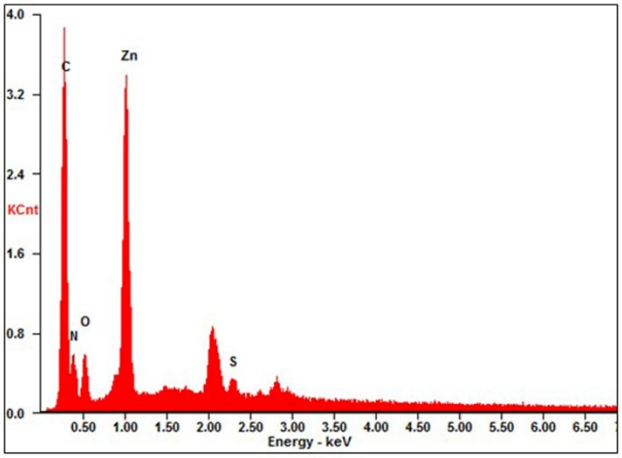

Fig. S13 EDX spectrum of AIZ NPs.

Table S2 Element percentages of AIZ NPs.

Materials	Zn (wt%)	N (wt%)	N/Zn
AIZ NPs	28.4	18.0	2.95

N/Zn(molar ratio) = (mass percentage of N / relative atomic mass of N) / (mass percentage of Zn/ relative atomic mass of N)

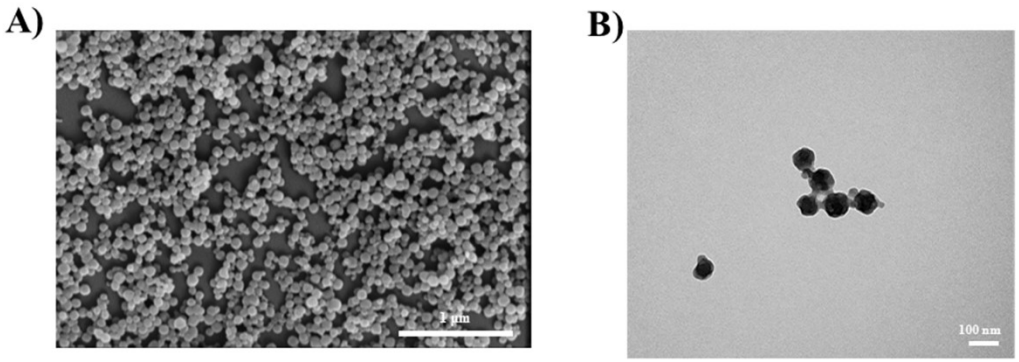

Fig. S14 A) SEM images of the ZIF-8. B) TEM images of the ZIF-8.

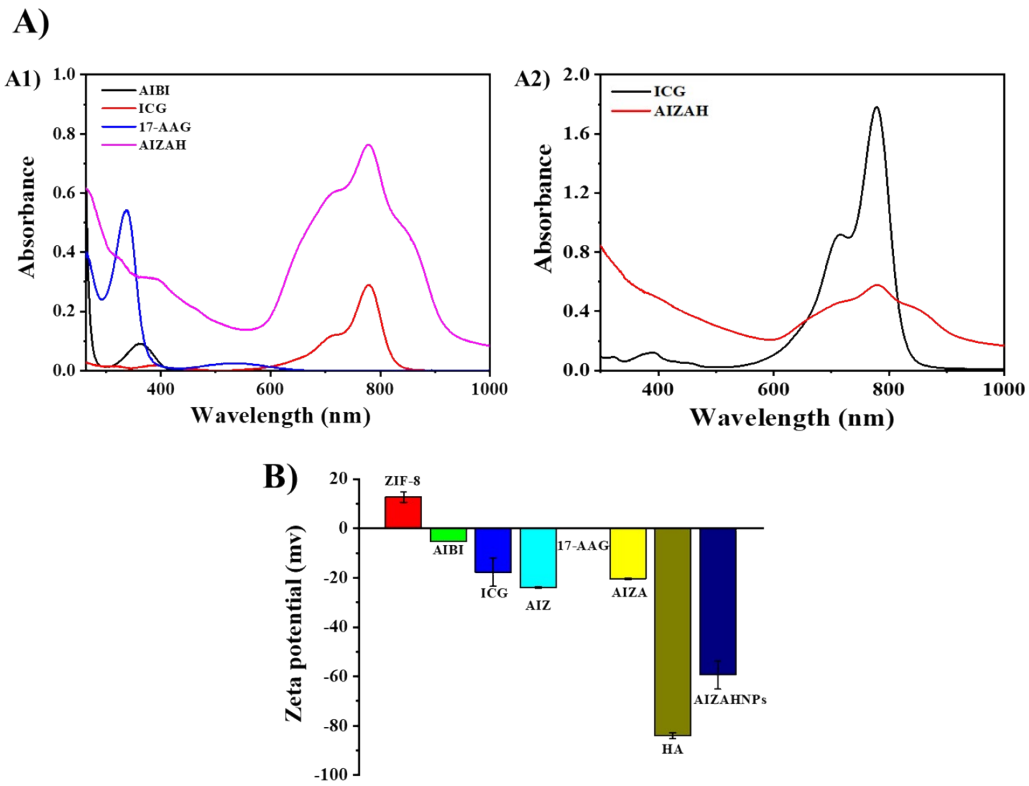

Fig. S15 A) A1)UV–vis absorption of ICG, AIBI ,17-AAG and AIZAH NPs. A2) UV–visible absorption spectra of ICG and AIZAH NPs NPs at the same equivalent concentration of ICG.(ICG:10.86μM) B) Zeta potential of ZIF-8, AIBI, ICG, AIZ NPs,17-AAG, AIZA NPs, HA and NPs. All data points represent as mean ± s.d. (n = 3).

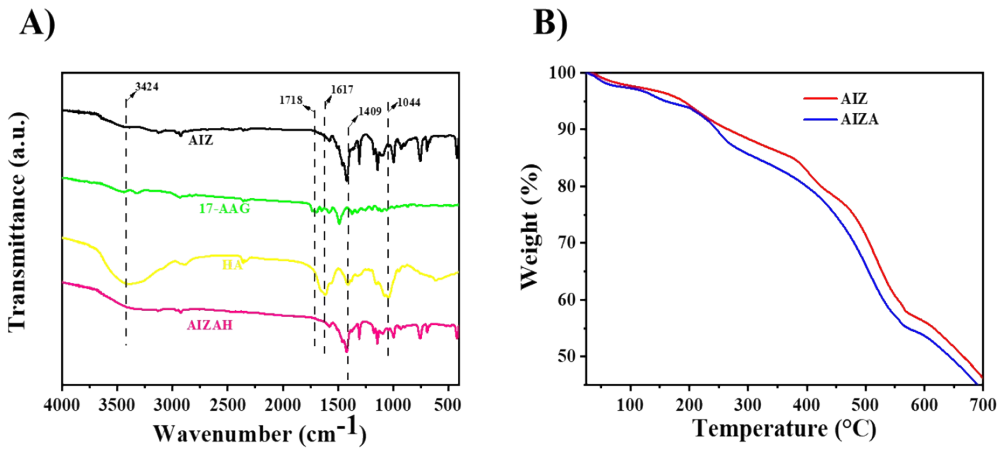

Fig. S16A) FT-IR spectra of AIZ NPs in comparison with that of AIZ NPs, 17-AAG,

HA and AIZAH NPs. B) TGA analysis of various samples.

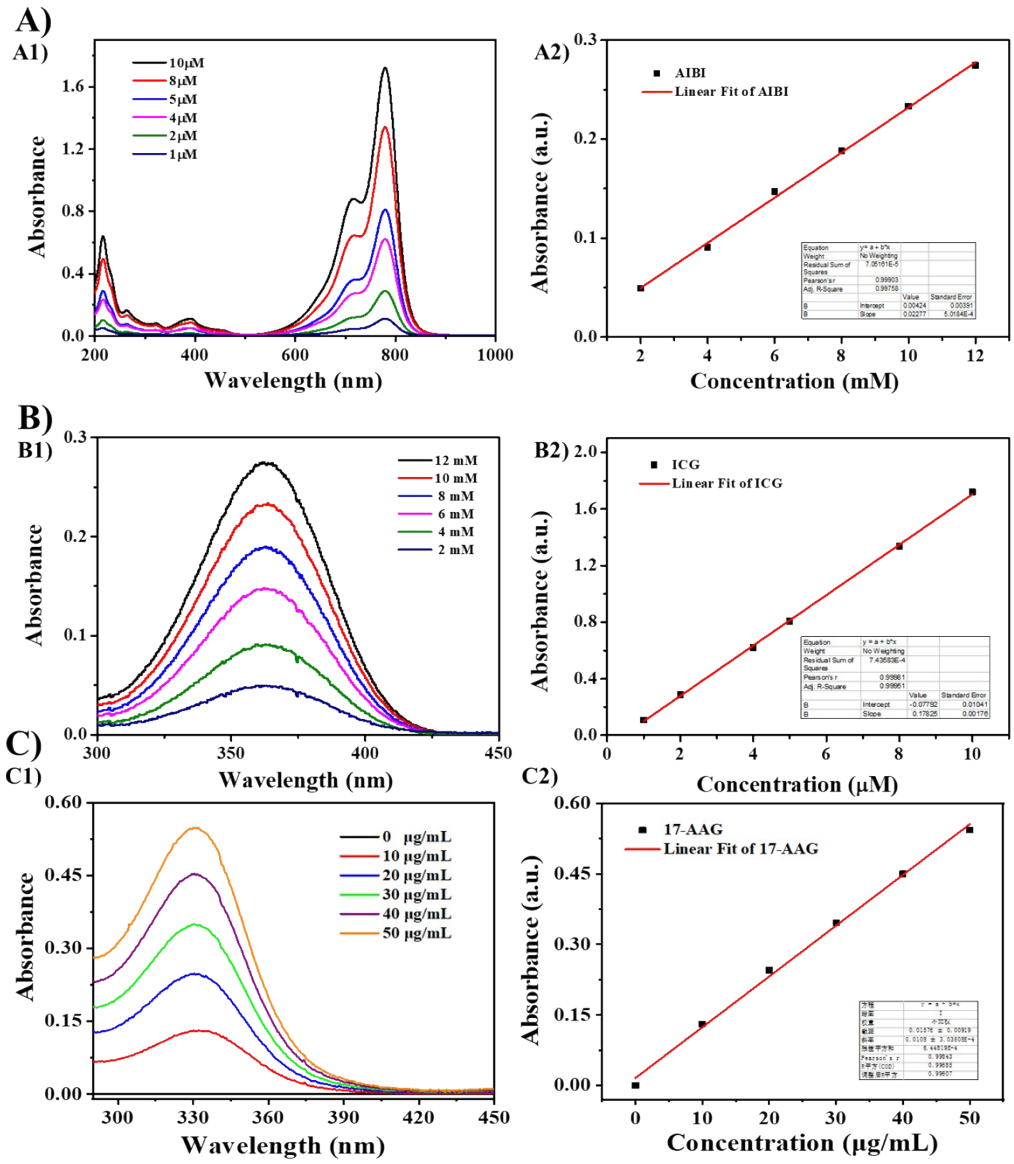

Fig. S17 A) A1) Standard absorbance curve of AIBI. A2) The absorbance of AIBI molecules at 363 nm (from water) as a function of AIBI concentration. B) B1) Standard absorbance curve of ICG. B2 The absorbance of ICG molecules at 779 nm (from water) as a function of ICG concentration. C) C1) Standard absorbance curve of 17-AAG. C2 The absorbance of 17-AAG molecules at 333 nm (from water) as a function of 17-AAG concentration.

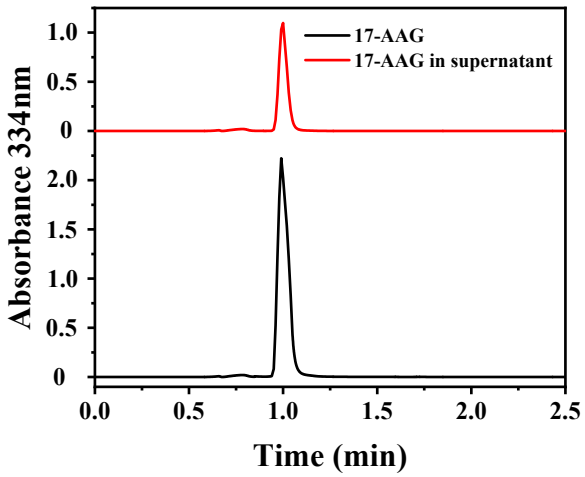

Fig. S18 UPLC of 17-AAG standard substance and 17-AAG in the supernatant.

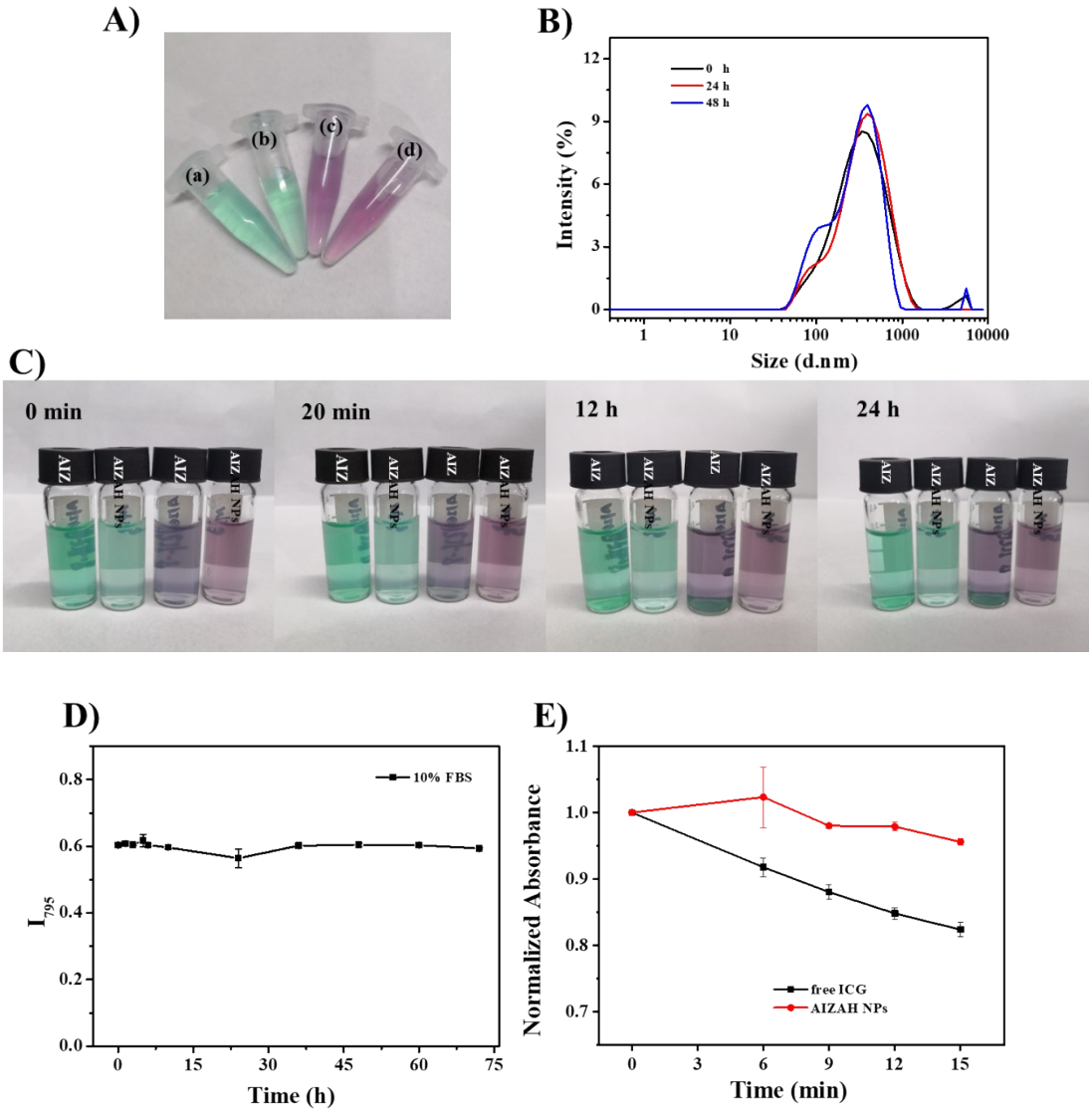

Fig. S19 A) Photographs of AIZAH NPs dispersed in a) DI water; b) PBS (pH 7.4); c) DMEM (without FBS); d) DMEM (with FBS). B) Size distributions measured by DLS of AIZAH NPs dispersed in PBS (pH 7.4) within 0 h, 24 h and 48 h. C) Digital photographs of AIZ NPs (200 μg/mL) and AIZAH NPs (200 μg/mL) dispersed in PBS (pH 7.4) (left) or RPMI Medium1640 (right) within 24 h. D) Stability of AIZAH NPs at 10% FBS. All data points represent as mean ± s.d. (n = 3). E) The thermal stability different compounds of AIZAH NPs, free ICG.

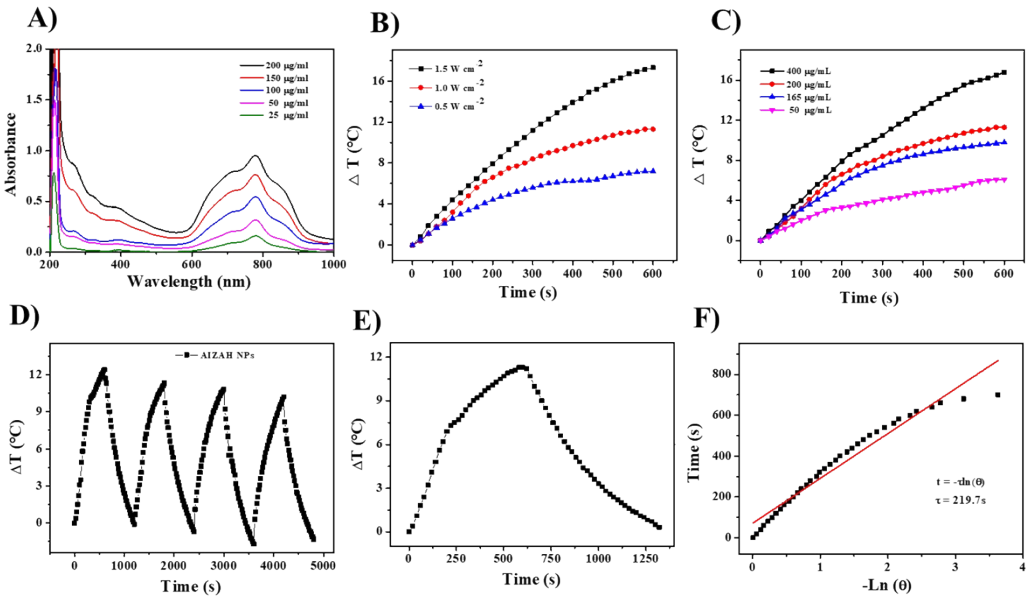

Fig. S20 A) UV–visible absorbance spectra of AIZAH NPs with different concentrations at room temperature. B) Temperature elevation curves of AIZAH NPs solution with gradient power densities (0.5, 1.0 and 1.5 W cm^{-2}) under 808 nm NIR irradiation for 600s. C) Temperature elevation curves of AIZAH NPs solution with gradient concentrations (50, 100, 165 and 150 μg/mL) under 808 nm NIR irradiation (1.0 W cm^{-2}) for 600s. D) Photothermal stability assay via 600 s laser exposure and 600 s cooling-down period. E) Photothermal effects of AIZAH NPs (200 μg/mL) under an 808 nm NIR irradiation (1.0 W cm^{-2}) for 600s and than stopping the irradiation. F) Linear fitting of time data versus -ln θ obtained from the cooling period of AIZAH NPs.

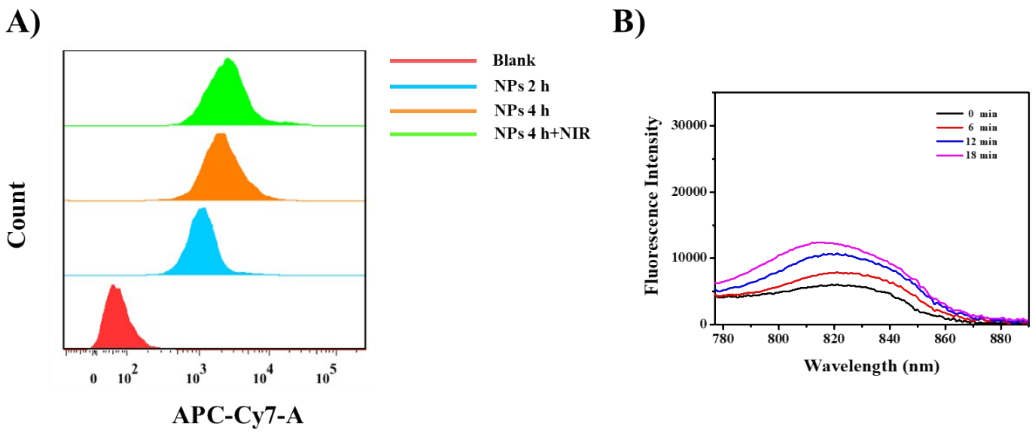

Fig. S21 A) Flow cytometry analysis of LNCaP cells after incubation with AIZAH NPs ([ICG] = 5 μg/mL) for 0 h, 2 h, 4 h, 4 h + NIR. B) Fluorescence intensity of AIZAH NPs under different laser time.

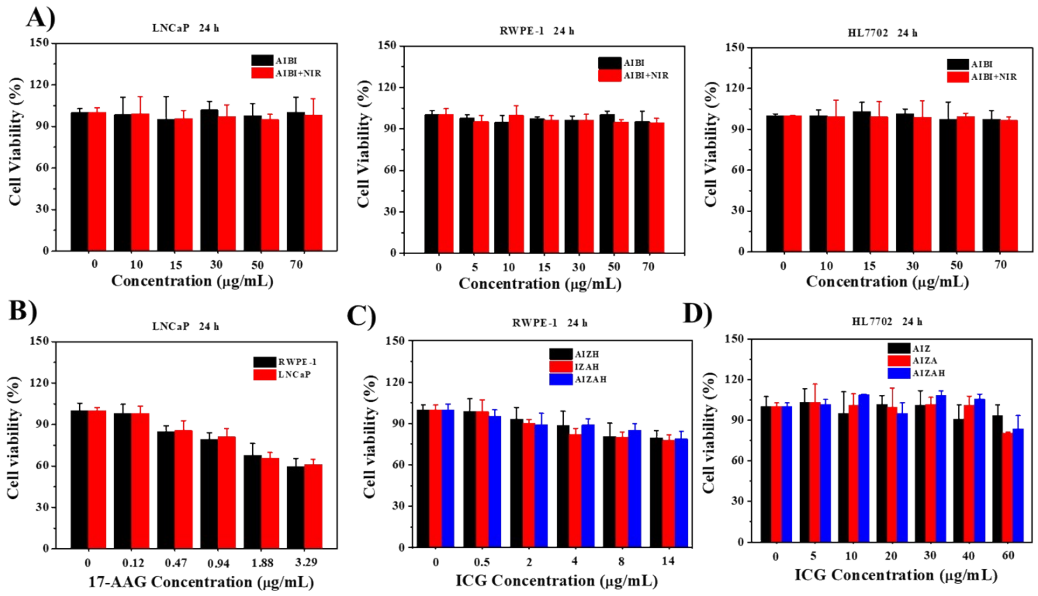

Fig. S22 A) Cell viability of LNCaP, RWPE-1 and HL7702 cells after 24 h in various samples with different concentrations and 10 minutes after NIR irradiation in the absence or presence of 808 nm laser (1.0 W cm^{-2}). B) Cell viability of LNCaP and RWPE-1 cells after 24 h in 17-AAG with different concentrations. Cell viability of C) RWPE-1 and D) HL7702 cells after 24 h in various samples with different concentrations. All data points represent as mean ± s.d. (n = 3).

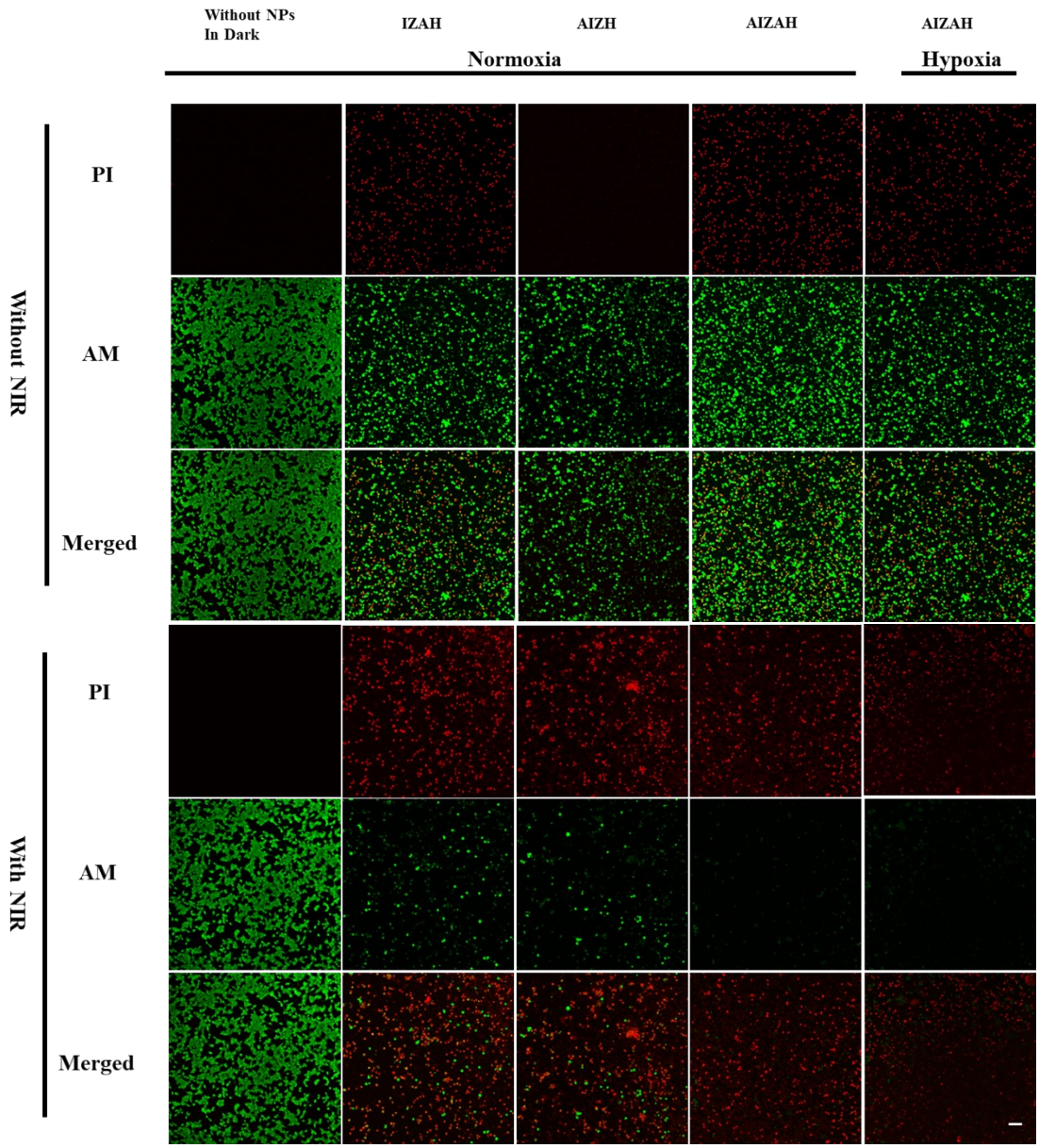

Fig. S23 Confocal fluorescence images of calcein AM/PI costained LNCaP cells after various treatments. Live and dead cells were stained with calcein AM and PI and presented in green and red colors, respectively. (Scale bar: 100 μm.)

Notes and References

1 B. Miehlich, A. Savin, H. Stoll and H. Preuss, *Chem. Phys. Lett.*, 1989, **157**, 200-206.

2 H. Zhang, W. Jiang, R. Liu, J. Zhang, D. Zhang and Z. Li, *ACS Appl. Mater. Interfaces*, 2017, **9**, 19687-19697.

3 W. Huang, J. Lin, J. Hsieh, S. Chou, C. Lai and E. Yun, *ACS Appl. Mater. Interfaces*, 2016, **8**, 30722-30734.